Self-Powered Triboelectric Nanosensor for Microfluidics and Cavity-Confined Solution Chemistry

Xiuhan Li,[†,‡,#] Min-Hsin Yeh,[#,†] Zong-Hong Lin,[†,§,#] Hengyu Guo,[†] Po-Kang Yang,[†] Jie Wang,[†] Sihong Wang,[†] Ruomeng Yu,[†] Tiejun Zhang,[†] and Zhong Lin Wang[*,†,⊥]

[†]School of Materials Science and Engineering, Georgia Institute of Technology, Atlanta, Georgia 30332, United States, [‡]School of Electronic and Information Engineering, Beijing Jiaotong University, Beijing 100044, China, [§]Institute of Biomedical Engineering, National Tsing Hua University, Hsinchu 30013, Taiwan, and [⊥]Beijing Institute of Nanoenergy and Nanosystems, Chinese Academy of Sciences, Beijing 100083, China. [#]X.L. and M.-H.Y. contributed equally to this work.

ABSTRACT Micro total analysis system (μTAS) is one of the important tools for modern analytical sciences. In this paper, we not only propose the concept of integrating the self-powered triboelectric microfluidic nanosensor (TMN) with μTAS, but also demonstrate that the developed system can be used as an *in situ* tool to quantify the flowing liquid for microfluidics and solution chemistry. The TMN automatically generates electric outputs when the fluid passing through it and the outputs are affected by the solution temperature, polarity, ionic concentration, and fluid flow velocity. The self-powered TMN can detect the flowing water velocity, position, reaction temperature, ethanol, and salt concentrations. We also integrate the TMNs in a μTAS platform to directly characterize the synthesis of Au nanoparticles by a chemical reduction method.

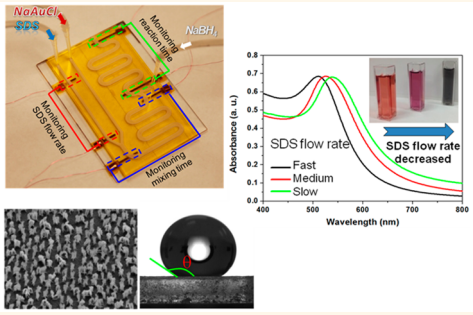

KEYWORDS: Au nanoparticles · micro total analysis system · microfluidics · self-powered sensor · triboelectric effect

Micro total analysis system (μTAS) or lab on a chip,[1] which was first developed more than 20 years ago, now has been recognized as an efficient analysis platform for biological, chemical, cellular, and nucleic acid analyses.[2] Because of the advantages of easy fabrication, low cost, and reduced amount of analytes and reactants,[3] μTAS has also been applied in environment science,[4,5] medicine development,[6,7] and nanoparticle synthesis.[8−10] However, most studies are only focused on the applications of μTAS but not on developing an integrated and self-powered nanosensor for *in situ* characterization of liquid characteristics and fluid flow mechanism.[11] This study is very important because the fluidic flow in μTAS is complex, which will be determined by the surface force and roughness of the microchannels.[12]

The conventional method to observe the fluidic flow in μTAS is through a microparticle image velocimetry system.[13] However, this kind of bulky and expensive equipment is composed of a microscope, CCD camera, light source, and circulating system,[14] which largely restricts its application. In addition, various μTAS platforms have been developed and proposed for different purposes and applications. So other microfluidic sensors based on acoustic,[15] thermal electric,[16] electromagnetic,[17] and electrostatic effects[18] have also been developed. Nevertheless, due to the complicated working principles and fabrication methods, they are not the best candidates as sensors in μTAS.

In recent years, many different types of nanogenerators[19−21] and self-powered nanosensors[22−26] based on the coupling of triboelectric and electrostatic effects have been demonstrated. The triboelectric charges generated during the contact and separation processes determine the performance of nanogenerators and self-powered nanosensors. Actually, not only can the solid−solid materials be used to compose the device, but scientists have also used the solid−liquid contact electrification to harvest the liquid energy and as self-powered sensors for static solution temperature, polarity, and salt concentration detections.[27−30] However, there are no reports mainly focusing on

* Address correspondence to zhong.wang@mse.gatech.edu.

Received for review July 20, 2015 and accepted October 15, 2015.

Published online 10.1021/acsnano.5b04486

the triboelectric effect between the flowing liquid and the nanomaterial in a μTAS and further introducing this kind of phenomenon as a signal source to monitor the several parameters in such system. Of most importance is the fact that triboelectric based device is very suitable for miniaturization and integration with any type of substrate, with a great potential as self-powered sensors in μTAS.

In this paper, the first self-powered triboelectric microfluidic nanosensor (TMN) is developed based on the working principle of single-electrode triboelectric nanogenerator. Our proposed self-powered TMN has been successfully demonstrated to detect the flowing water velocity, droplet position, reaction temperature, ethanol and salt concentrations. The simulation results support the proposed working mechanism of TMN. We also integrated the TMN in a μTAS platform to directly characterize the synthesis of Au nanoparticles by a chemical reduction method. Results show that the concept of TMN has the potential to become a key technological solution for realizing a self-powered μTAS.

RESULTS AND DISCUSSION

The integrated device containing TMN and μTAS is schematically illustrated in Figure 1a. Basic units of substrate (poly(methyl methacrylate), PMMA), electrode (Cu thin film), and triboelectric layer/contact material (Kapton nanofilm) are used to compose the TMN. The fabrication process is shown in Figure S1. The surface of triboelectric layer is fabricated as nanostructures in order to increase the hydrophobicity (Figure 1b). The nanostructures were formed through reactive ion etching. Figure 1c clearly shows the nanostructures on the surface are nanowire arrays. To optimize the tribo-charges generated during the solid−water contact electrification, we further coated 1*H*,1*H*,2*H*,2*H*-perfluorodecyltriethoxysilane (PTFS) on the surface.[31] The contact angle measured from Figure 1d is 152°,

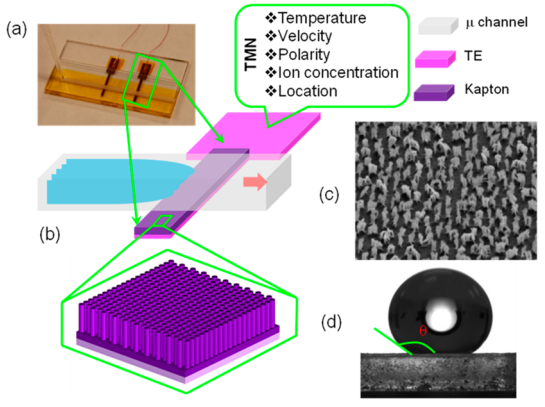

Figure 1. 3D schematic of TMN integrated with microchannel (μC): (a) μC with two TMNs distributed. (b) Structure illustration of TMN (composed by TE (tribo-elelectrode) and Kapton nanostructure) and μC. (c) SEM image of Kapton nanostructure. (d) Contact angle of the Kapton surface.

which can be used to define the surface of Kapton film finally as superhydrophobic. The fabrication of the microfluidic chip is facile and highly reproducible. We have fabricated over 20 devices and confirm the reproducibility. For each device, the fluctuation in electrical outputs for sensing targets is less than 10%.

The working principle of the TMN relies on the coupling between contact electrification and electrostatic induction as caused by the approaching and departing of the fluidic drop, which is the driving force causing the electron exchange between the tribo-electrode and the ground. This phenomenon was explained by using an interfacial electrical double-layer model, which took into account the ions in the liquid adsorbed onto the solid surface.[20,28,29] The mechanism of how TMN can be used to detect the liquid characteristic is shown in Figure 2. Figure 2a,b shows the photographs for the fluid before and after passing the TMN. First, the triboelectric layer (Kapton) was treated with water to ionize its surface with negative charges. To maintain the electroneutrality, positive charges were induced on tribo-electrode (Cu) *via* electrostatic introduction (Figure 2c). Once the liquid enters into contact with the triboelectric layer, positive charges (such as hydroxonium ions) in water can screen the negative charges on the triboelectric layer by forming an interfacial electrical double layer. Meanwhile, due to the unbalanced charge distribution between the triboelectric layer and tribo-electrode, the unbalanced positive tribo-potential builds up and then drives the electrons to flow from the ground to the tribo-electrode in order to balance the potential difference (Figure 2d) until reaching an equilibrium state (Figure 2e). On the other hand, numerical calculations of the tribo-potential distribution across the tribo-electrodes of the TMN under open-circuit condition were also evaluated by COMSOL and the results are shown in Figure 2f,g. Before the liquid contacts the triboelectric layer, there is no potential difference on the tribo-electrode (Figure 2f), which is identical as we describe in Figure 2c. Once the fluid passes through the TMN, the positive charges in the water will neutralize the negative charges in triboelectric layer, which could induce a positive tribo-potential between the tribo-electrode and the ground and then drive the electrons to flow from the ground to the tribo-electrode (Figure 2g) until reaching an equilibrium state (Figure 2h). These results indicate that the fluid passing through the TMN will cause the electrons to flow from the ground to the tribo-electrode, creating current and voltage signals.

To characterize the generated outputs from the TMN in μTAS, a syringe pump, whose input volume flow rate (V_{pump}) can be controlled from milliliters per second to nanoliters per second (mL/s to nL/s), is applied to drive the liquid flowing in the microfluidic channels. The half wave sine output short circuit current and open circuit

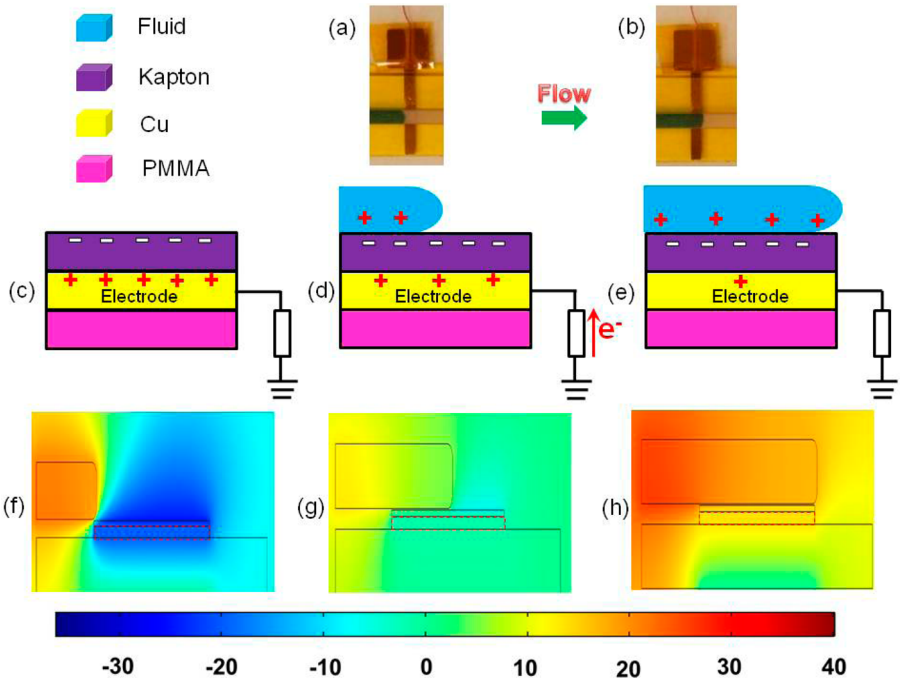

Figure 2. Working mechanism of TMN: (a and b) photographs for the fluid before and right after passing the TMN. Before the liquid passes the TMN, as Kapton layer contains negative charges after water ionization, positive charges are induced on the electrode due to electrostatic induction. (c) Once the liquid starts to contact the triboelectric layer (Kapton), positive charges in fluid will neutralize the negative charges in the Kapton layer and this will cause the electrons to flow from the ground to the electrode (d) and finally reach the equilibrium (e). (f and g) Calculated results of the tribo-potential distribution across the tribo-electrodes of the TMN under open-circuit condition.

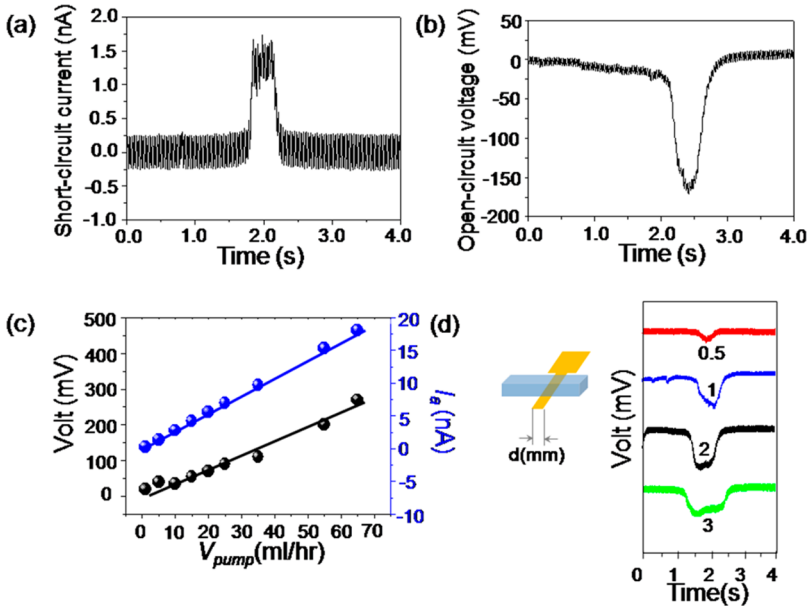

Figure 3. Output short-circuit current (a) and open-circuit voltage (b) as tap water is passing through the TMN. (c) The relationship between the generated outputs and flow rate of tap water. (d) The relationship between the width of output voltage and the width of the electrode (d).

voltage as tap water only passing through the TMN are shown in Figure 3a,b. The output current and voltage amplitude are around 5 nA and 150 mV, respectively. Also, the short-circuit current and the open-circuit voltage are in opposite directions, implying that the TMN is acting not only as a sensor in μTAS, but also as a power source to drive itself to fully realize the self-powered nanosystem. As the generated power from TMN is not high enough to drive the measuring system, we can integrate another triboelectric nanogenerator to power the measuring system and build up a self-powered TMN system. Next, we studied the relationship

between the generated outputs and the volume flow rate from the injection pump (V_{pump}) which is consistent with the *in situ* flow velocity (v_f) of tap water in the microchannel. When the volume flow rate from the pump (V_{pump}) is increased from 5 to 65 mL/h, the output current amplitude (I_a) and voltage amplitude (Volt) can be enhanced from 2.5 to 17 nA and from 5 to 250 mV, respectively (Figure 3c). The results clearly show both the output current amplitude (I_a) and the voltage are increased with the pump volume flow rate (V_{pump}). The increase of I_a and Volt is because the contact electrification between the liquid and TMN is enhanced with the liquid flow rate.[32] Eric *et al.*[33] derived the relationship between the current caused by contact electrification and the average flow velocity, which indicates that the induced current is proportional to the flow velocity; meanwhile, the contact induced tribo-charge quantity is also increased.[29] So the corresponding output current and voltage are both increased with the liquid flow rate as shown in Figure 3c. The dependence of output voltage on the passing path d (0.5, 1, 2, and 3 mm) of TMN is shown in Figure 3d. The longer the passing path d of TMN is, the broader the output signal that is obtained. This can be explained as the time of the tap water contacting with the TMN, as shown in Figure 3d: it will take longer time for tap water passing through the TMN if the width of the electrode is wider, leading to an increase in the width of the generated voltage pulse. The longer the passing path d of TMN is used, the broader the output signal that is obtained. This can be explained as the time of the tap water contacting with the TMN.

Compared to the macrosystems, the fluid dynamics in microfluidic channels are more complex. For example, the surface tension needs to be reevaluated in microfluidic channels.[34] Hence, how to acquire the *in situ* flow velocity (v_f) in microfluidic channels has become a serious issue in related research.[35] In this part, we integrated different numbers of triboelectric nanosensors along the same microfluidic channels in order to investigate the system in depth. In this system, the *in situ* flow velocity (v_f) can be calculated through the distance (l) and the time interval (t_i) of the fluid traveling between the two TMNs. The distance (l) between the two TMNs is designed to be 4 cm. The times when the fluid is reaching TMN_1 and TMN_2 are t_1 and t_2. So the *in situ* flow velocity of fluid (v_f) in microchannels can be obtained through measuring the time interval ($t_i = t_2 - t_1$) of the outputs from the two triboelectric nanosensors. The *in situ* flow velocity (v_f) of fluid in microchannels can be calculated as

$$v_f = \frac{l}{t_i} \quad (1)$$

It can be used to calculate the *in situ* flow velocity of fluid in different microfluidic channels. The demonstration of measuring different flow velocity of fluids is

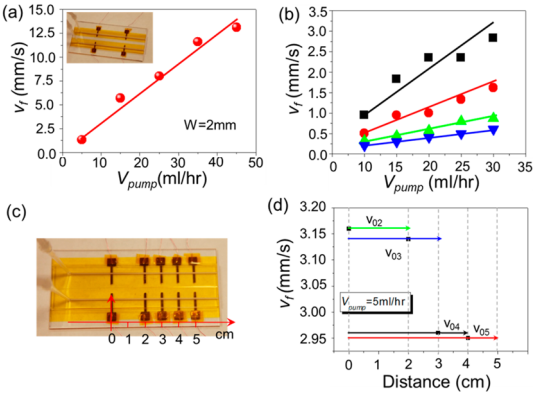

Figure 4. Two TMNs are used to measure the *in situ* flow velocity in the μC. (a) Relationship between the *in situ* flow velocity v_f and the pump volume flow rate V_{pump}. (b) The channel resistance (f) measured and with results compared for different microfluidic channels. (c) TMN network composed of five TMNs is distributed in microfluidic channels. (d) The average flow velocity measurement in microfluidic channel by TMN network.

shown in Supporting Information (Video S1). After the calculations, the higher *in situ* flow velocity (v_f) of fluid in microchannel is 6.3 mm/s and the slower one is 3.9 mm/s.

Figure 4a shows the input volume flow rate of fluid from the pump (V_{pump}) and the *in situ* flow velocity (v_f) of fluid we measured in the microchannels. The width of microchannel is 2 mm and the electrode width for TMN is 1 mm. To correct the difference between the results obtained in those two approaches, we introduce the coefficient of channel resistance f_c and the cross section area S of the microchannel in a relationship between v_f and V_{pump} as given by

$$v_f = \frac{f_c V_{pump}}{S} \quad (2)$$

The fluid flowing in microchannels is quite different from that in macrochannels. As the surface roughness and the dimensions of microchannel have great impact on the flow dynamics; there are many factors that will determine the channel resistance (f) in microchannels.[36,37] How to measure and compare the channel resistance in different microchannels is an important issue in related research application. Microchannels with a rectangular cross section are designed for the measurement and comparison (Figure S2); is the length of the cross section is b and the width is a, the equivalent diameter d_e of microchannel with rectangular cross section is

$$d_e = \frac{2ab}{a+b} \quad (3)$$

The relationship between the volume flow rate V_{pump} and the *in situ* flow velocity (v_f) in microchannel is

$$v_f = f_c \frac{V_{pump}}{a \times b} \quad (4)$$

Here f_c is the channel resistance coefficient caused by the liquid passing the microchannel with different cross section area ($S = a \times b$).

The Reynolds number (*Re*) can be obtained through the following equation:

$$Re = \frac{\rho v_f d_e}{\mu_f} \quad (5)$$

Here μ_f is the viscosity, ρ is the density of the flowing liquid, v_f is the *in situ* flow velocity in microchannel, and d_e is the equivalent diameter calculated from eq 3. For the microchannel scale, *Re* is smaller than 2300 and belongs to Laminar flow; the channel resistance *f* can be obtained from

$$f = \frac{64}{Re} \quad (6)$$

Hence, the channel resistance (*f*) in the microchannel can be deduced from eqs 3−6)

$$f = \frac{32\mu_f(a+b)}{\rho f_c V_{pump}} \quad (7)$$

The value of channel resistance (*f*) for microfluidic channels can also be measured and compared through analyzing the output signal from TMNs network. From eq 7, assume the height *b* of the microfluidic channels is at the same value because of the consistent microfabrication method, it can be concluded that the channel resistance (*f*) for microfluidic channels changes linearly with the channel width at the same V_{pump}. Moreover, from eqs 4 and 7) for the same channel, the *in situ* flow velocity (v_f) changes linearly with V_{pump} as shown in Figure 4b. Figure 4b also compares the relationship between V_{pump} and v_f in microfluidic channels with different width (0.5, 1.0, 2.0, and 3.0 mm). The channel resistance of each microfluidic channel can be obtained through the slope (K_c) of the curve for different channel with different widths:

$$\frac{1}{f} = \frac{\rho f_c V_{pump}}{32\mu_f(a+b)} = K_c V_{pump} \quad (8)$$

Through this method, the channel resistance (*f*) for microfluidic channels can be easily obtained and compared. Microfluidic channel with the width of 0.5 mm has the largest value of *f* and the flow velocity change most slowly comparing with the microfluidic channel with larger width. Hence, the TMN can be used to measure the *in situ* channel resistance and control the flow velocity in different microfluidic channels. It can further be used to control the molar ratio of cosolvents, mixing and reaction time for μTAS.

Several TMNs can be arranged along the microfluidic channels to act as the flow velocity and liquid location measurement sensor network as shown in Figure 4c, such as TMN_0, TMN_2, TMN_3, TMN_4, and TMN_5. The distances between the adjacent sensors are l_{02} (2 cm), l_{03} (3 cm), l_{04} (4 cm), and l_{05} (5 cm). The average flow velocity between TMN_0 and TMN_2, TMN_3, TMN_4, and TMN_5 is v_{02}, v_{03}, v_{04}, and v_{05} and can be measured and calculated through eq 1. Figure 4d is the average flow velocity for different time intervals in the microfluidic channel. The relationship between the average flow velocity is $v_{02} > v_{03} > v_{04} > v_{05}$. Hence, it can be used to analyze the flow stability in microfluidic channel and there is a velocity difference in the microchannels at different test interval. This is because the channel resistance (*f*) for microfluidic channel increased with the length (*l*) of the microfluidic channel, just like the relationship between the resistance and the resistor length. Hence, the average flow velocity in the same microfluidic channel is decreasing with the value of *l* for the increase of channel length (Figure 4d). The TMN networks can be used to measure the *in situ* flow velocity and detect the location of micro flow in μTAS.

Previous studies have shown the generated tribo-potential from solid−water contact electrification is sensitive to the solution polarity, temperature, and ion concentration.[27−30] However, all those results are obtained in macrosystems. In our study, we first observed the generated outputs of triboelectric nanosensors when the solutions containing different concentrations of ions (Figure 5a). We chose deionized water and tap water as our samples. When deionized water is used, the output voltage of TMN can increase from 25 to 150 mV as the pump volume flow rate (V_{pump}) of deionized water varies from 5 to 65 mL/h, which is much higher than that obtained by using tap water. The results indicate the generated outputs from triboelectric nanosensors will be affected by the concentrations of ions in the solution. This is because the positive ions in the solution will be adsorbed on the Kapton film (with negative charges on the surface) to form electrical double layer (EDL) and screen the tribo-potential.[28] Hence, higher generated outputs from triboelectric nanosensors will be obtained when using deionized water instead of tap water. Figure 5b shows that the output voltage is also affected by the concentration of $NaAuCl_4$.The generated voltage amplitude (Volt) is decreasing with the concentration of $NaAuCl_4$ at the same V_{pump}. As increasing the concentration of $NaAuCl_4$ will increase the positive charge density in the flowing liquid, the tribo-charges on the Kapton film will decrease and the corresponding generated voltage will decrease.[20] When the concentration of $NaAuCl_4$ changed from 25 μM to 25 mM, the generated voltage changed from 350 to 150 mV. The generated voltage decreased with the concentration of $NaAuCl_4$ linearly at the pump rate of 5 mL/h. This is very important for the Au nanoparticles synthesizing μTAS, which can be used to control the results of the chemical reaction.

Figure 5c represents the output voltage of the TMN when the liquid containing different concentrations of ethanol passes it. As the concentration of ethanol in water varied from 0 to 20%, the output voltage was decreased from 200 to 100 mV. The decrease of voltage

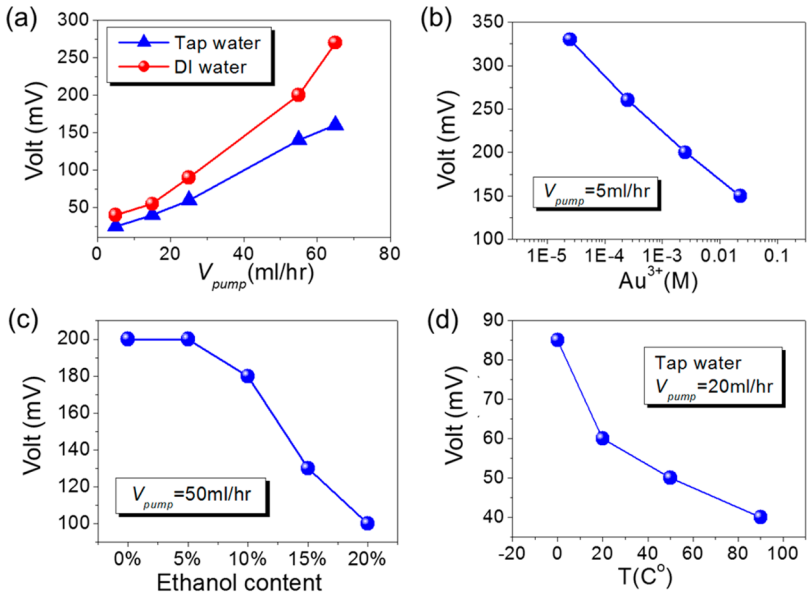

Figure 5. TMN can be used as chemical sensors: (a) the generated voltage amplitude Volt *vs* the water type; (b) Volt *vs* the concentration of $NaAuCl_4$; (c) Volt *vs* the content of ethanol; (d) Volt *vs* the reaction temperature of flowing liquid.

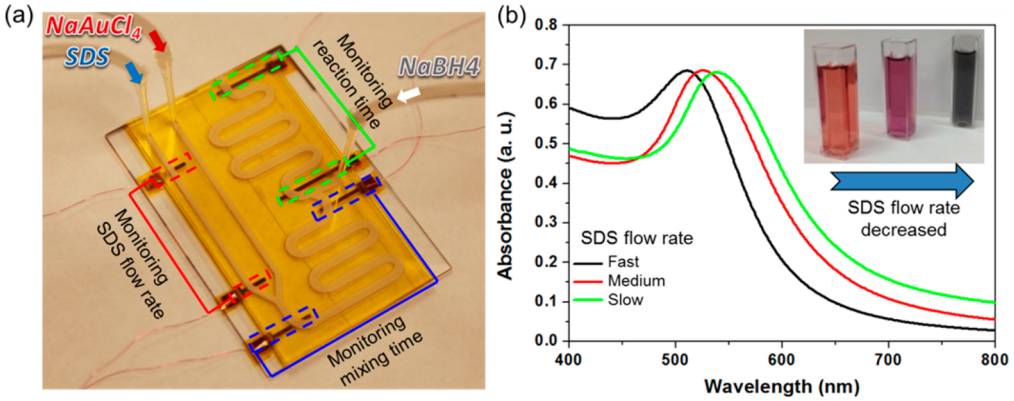

Figure 6. (a) Micro Total Analysis System (μTAS) with six TMNs for Au nanoparticle synthesizing; (b) Au nanoparticle size detected by UV−vis absorption spectrum.

is because of the presence of ethanol that screens the tribo-charges generated during the solid−water contact electrification. Another important factor to influence the output of TMN is the water temperature. When the temperature of flowing water changed from 0 to 90 °C, the output voltage was decreased from 85 to 40 mV (Figure 5d). The presence of ethanol in water or increase of water temperature could cause the decrease of generated outputs from TMN because they will decrease the water polarity and, consequently, enhance the interaction with the Kapton film.[38] Therefore, when the fluid is passing through the triboelectric nanosensor, water will not separate from the Kapton film very effectively and affect the quantity of tribo-charges generated during the process.

In the final part, we demonstrate that the integration of triboelectric nanosensors with μTAS can be applied in monitoring the synthesis of Au nanoparticles. Figure 6a is the photograph of the fabricated μTAS that consists of multiple triboelectric nanosensors with different sensing functions in this system. The sensing targets include the flow rate of surfactant sodium dodecyl sulfate (SDS) solution, mixing time of $NaAuCl_4$ and SDS solution, and reaction time for Au nanoparticles formation. The *in situ* monitoring of the reaction is shown in Supporting Information (Video S2). In the applications of Au nanoparticles, the size of Au nanoparticles is a critical issue because it will affect many properties, like the absorption of surface plasmon resonance and catalytic activity. Therefore, we also discussed the important factor that could affect the size of synthesized Au nanoparticles in our proposed TMN based μTAS. A previous study has reported that the size of Au nanoparticles can be tuned by varying the surfactant concentration.[39] This is because the surfactant concentration will determine the micelle size and shape, which is used to stabilize and control the growth of Au nanoparticles. We used the injection pump to control the flow rate of SDS solution. So when the flow velocity of SDS solution is fast, there will be

more SDS present when later $NaAuCl_4$ is reduced by $NaBH_4$. Figure S3 shows the well-mixed $NaAuCl_4$ and SDS solution after both of them have passed through the micro mixing nozzle, which represents the high quality of the fabricated μTAS. After the characterization by UV−vis absorption spectrum (Figure 6b) and transmission electron microscopy (Figure S4), we found the size of Au nanoparticles is highly related to the flow velocity of SDS solution. We further optimized three different flow rate of SDS solution to synthesize 15, 30, and 55 nm Au nanoparticles. All of the results verify that the fabricated μTAS with integrated triboelectric nanosensors can be used to detect the different reaction conditions in the system and control the products. Therefore, we believe that this fabrication method and TMN has great application potential in μTAS. This concept will not be limited to the chemical synthesizing system, it also has the potentials to be applied in other μTAS.

CONCLUSION

In summary, a novel TMN has been developed for microfluidic flow velocity measurement and fluid position detection. It has been demonstrated that the electric current amplitude (I_a) and voltage (Volt) generated when the flowing liquid passes the TMN change linearly with the flow velocity. Several TMNs can cooperate with each other to measure the *in situ* flow velocity and stability in micro flow. The TMN also acts as self-powered chemical sensor to characterize the temperature, concentration of metal ion, and the polarity parameter of the reaction liquid online in μTAS, which can be utilized to control the results of the chemical reactions. The TMNs can be easily integrated with microfluidic channels and μTAS through the batch fabrication method. Therefore, on the basis of the above results, a self-powered μTAS platform with TMN sensor network was built in an Au nanoparticle synthesizing setup to control several experimental parameters, *i.e.*, concentration of $NaAuCl_4$ solution, molar ratio of cosolvents, reaction temperature, flow velocity, mixing and reaction time. The results indicate that the TMN and its sensor network has great potential for microfluidics application and associated kinetics control in chemical reactions.

METHODS

Superhydrophobic Surface Treatment by LAH and PTFS. To meet the microfluidics application, the surface of the microfluidic channel must be super hydrophobic; therefore, the surface modification is applied on the PMMA substrate. First, after a cleaning step using DI water and ethyl alcohol, the PMMA microfluidic substrate was put in 4 M lithium aluminum hydride (LAH) for 24 h.[40] Then, the substrate was deeply cleaned in ultrasonic cleaning machine. After that, the substrate was immersed in a solution of 1*H*,1*H*,2*H*,2*H*-perfluorodecyltriethoxysilane (PFTS) in diethyl ether (5% v/v) for 1 h. Finally, the substrate was rinsed thoroughly with 2-propanol and then cured in a vacuum oven at 80 °C for 10 h.

RIE Etching of the Kapton Nanostructure. To create the nanowire structures on the surface of the Kapton thin film (50 μm), an induced coupled plasmon (ICP) reactive ion-etching technique was used. Specifically, Ar, O_2, and CF_4 gases were introduced into the ICP chamber with the flow rate of 15.0,10.0, and 30.0 sccm, respectively. One power source of 400 W was used to generate a large density of plasma, and the other power of 100 W was used to accelerate the plasma ions. The Kapton thin film was etched for 5 min, and the length of the as-fabricated nanowire array ranged from 0.4 to 1.1 μm. One power source of 400 W was used to generate a large density of plasma, and the other power of 100 W was used to accelerate the plasma ions.

Characterization. A Hitachi SU8010 field emission scanning electron microscope (SEM) was used to measure the size and height of NS on Kapton film. In the electric output measurement of the TMN, an injection pump was used to provide uniform volume flow rate for sensor performance characterization. For the measurement of electrical outputs of TENG, a programmable electrometer (Keithley model 6514) and a low noise current preamplifier (Stanford Research System modelSR570) were used. Contact angle was measured in clean room. The size of as-prepared Au nanoparticles were examined by transmission electron microscopy (JEOL, TEM-1230).

Conflict of Interest: The authors declare no competing financial interest.

Supporting Information Available: The Supporting Information is available free of charge on the ACS Publications website at DOI: 10.1021/acsnano.5b04486.

More detailed information about the fabrication method for TMN integrated with microchannel and chip including the process steps and the SEM and optical image for planarization and micro mixer; TEM measurement results for the Au nanoparticle size under different flow rate of SDS solution (PDF)
Video S1: two channels (WMV)
Video S2: Au synthesis utas (WMV)

Acknowledgment. This work was supported by Hightower Chair foundation, the "thousands talents" program for pioneer researcher and his innovation team, China, Beijing City Committee of science and technology project (Z131100006013004 and Z131100006013005), Beijing National Science Foundation (4122058), Beijing Higher Education Young Elite Teacher Project (YETP0536), National Natural Science Foundation of China (60706031 and 61574015), the Fundamental Research Funds for the Central Universities (2014JBM009) and Taiwan Ministry of Science and Technology (103-2113-M-007-021-MY2 and 103-2917-I-564-070). Patents have been filed based on the research presented here.

REFERENCES AND NOTES

1. Whitesides, G. M. The Origins and the Future of Microfluidics. *Nature* **2006**, *442*, 368–73.
2. Manz, A.; Graber, N.; Widmer, H. M. Miniaturized Total Chemical Analysis Systems: A Novel Concept for Chemical Sensing. *Sens. Actuators, B* **1990**, *1*, 244–248.
3. Craighead, H. Future Lab-on-a-Chip Technologies for Interrogating Individual Molecules. *Nature* **2006**, *442*, 387–93.
4. Marle, L.; Greenway, G. M. Microfluidic Devices for Environmental Monitoring. *TrAC, Trends Anal. Chem.* **2005**, *24*, 795–802.
5. Li, H. F.; Lin, J. M. Applications of Microfluidic Systems in Environmental Analysis. *Anal. Bioanal. Chem.* **2009**, *393*, 555–567.
6. Kang, L.; Chung, B. G.; Langer, R.; Khademhosseini, A. Microfluidics for Drug Discovery and Development: From Target Selection to Product Lifecycle Management. *Drug Discovery Today* **2008**, *13*, 1–13.

7. Liu, C.; Wang, L.; Xu, Z.; Li, J.; Ding, X.; Wang, Q.; Chunyu, L. A Multilayer Microdevice for Cell-Based High-Throughput Drug Screening. *J. Micromech. Microeng.* **2012**, *22*, 065008.
8. Navin, C. V.; Krishna, K. S.; Theegala, C. S.; Kumar, C. S. S. R. Lab-on-a-Chip Devices for Gold Nanoparticle Synthesis and Their Role as a Catalyst Support for Continuous Flow Catalysis. *Nanotechnol. Rev.* **2014**, *3*, 39–63.
9. Li, Y.; Sanampudi, A.; Raji Reddy, V.; Biswas, S.; Nandakumar, K.; Yemane, D.; Goettert, J.; Kumar, C. S. Size Evolution of Gold Nanoparticles in a Millifluidic Reactor. *ChemPhysChem* **2012**, *13*, 177–82.
10. Krishna, K. S.; Li, Y.; Li, S.; Kumar, C. S. Lab-on-a-Chip Synthesis of Inorganic Nanomaterials and Quantum Dots for Biomedical Applications. *Adv. Drug Delivery Rev.* **2013**, *65*, 1470–95.
11. Fiorini, G. S.; Chiu, D. T. Disposable Microfluidic Devices: Fabrication, Function, and Application. *BioTechniques* **2005**, *38*, 429–446.
12. Haeberle, S.; Zengerle, R. Microfluidic Platforms for Lab-on-a-Chip Applications. *Lab Chip* **2007**, *7*, 1094–110.
13. Kinoshita, H.; Kaneda, S.; Fujii, T.; Oshima, M. Three-Dimensional Measurement and Visualization of Internal Flow of a Moving Droplet Using Confocal Micro-Piv. *Lab Chip* **2007**, *7*, 338–46.
14. Lindken, R.; Rossi, M.; Grosse, S.; Westerweel, J. Micro-Particle Image Velocimetry (Micropiv): Recent Developments, Applications, and Guidelines. *Lab Chip* **2009**, *9*, 2551–67.
15. Abd Rahman, M. F.; Nawi, M. N. M.; Abd Manaf, A.; Arshad, M. R. Characterization of Microfluidic-Based Acoustic Sensor for Immersion Application. *IEEE Sens. J.* **2015**, *15*, 1559–1566.
16. Kopparthy, V. L.; Tangutooru, S. M.; Nestorova, G. G.; Guilbeau, E. J. Thermoelectric Microfluidic Sensor for Bio-Chemical Applications. *Sens. Actuators, B* **2012**, *166—167*, 608–615.
17. Zougagh, M.; Rios, A. Micro-Electromechanical Sensors in the Analytical Field. *Analyst* **2009**, *134*, 1274–1290.
18. Waggoner, P. S.; Craighead, H. G. Micro- and Nanomechanical Sensors for Environmental, Chemical, and Biological Detection. *Lab Chip* **2007**, *7*, 1238–55.
19. Wang, Z. L. Triboelectric Nanogenerators as New Energy Technology for Self-Powered Systems and as Active Mechanical and Chemical Sensors. *ACS Nano* **2013**, *7*, 9533–9557.
20. Zhu, G.; Su, Y.; Bai, P.; Chen, J.; Jing, Q.; Yang, W.; Wang, Z. L. Harvesting Water Wave Energy by Asymmetric Screening of Electrostatic Charges on a Nanostructured Hydrophobic Thin-Film Surface. *ACS Nano* **2014**, *8*, 6031–6037.
21. Zhu, G.; Peng, B.; Chen, J.; Jing, Q.; Lin Wang, Z. Triboelectric Nanogenerators as a New Energy Technology: From Fundamentals, Devices, to Applications. *Nano Energy* **2015**, *14*, 126–138.
22. Wang, Z. L. Self-Powered Nanosensors and Nanosystems. *Adv. Mater.* **2012**, *24*, 280–285.
23. Wang, Z. L. Triboelectric Nanogenerators as New Energy Technology and Self-Powered Sensors - Principles, Problems and Perspectives. *Faraday Discuss.* **2014**, *176*, 447–458.
24. Wang, S.; Lin, L.; Wang, Z. L. Triboelectric Nanogenerators as Self-Powered Active Sensors. *Nano Energy* **2015**, *11*, 436–462.
25. Li, X.; Lin, Z.-H.; Cheng, G.; Wen, X.; Liu, Y.; Niu, S.; Wang, Z. L. 3d Fiber-Based Hybrid Nanogenerator for Energy Harvesting and as a Self-Powered Pressure Sensor. *ACS Nano* **2014**, *8*, 10674–10681.
26. Yang, P. K.; Lin, L.; Yi, F.; Li, X.; Pradel, K. C.; Zi, Y.; Wu, C. I.; He, J. H.; Zhang, Y.; Wang, Z. L. A Flexible, Stretchable and Shape-Adaptive Approach for Versatile Energy Conversion and Self-Powered Biomedical Monitoring. *Adv. Mater.* **2015**, *27*, 3817.
27. Lin, Z. H.; Zhu, G.; Zhou, Y. S.; Yang, Y.; Bai, P.; Chen, J.; Wang, Z. L. A Self-Powered Triboelectric Nanosensor for Mercury Ion Detection. *Angew. Chem., Int. Ed.* **2013**, *52*, 5065–5069.
28. Lin, Z. H.; Cheng, G.; Lin, L.; Lee, S.; Wang, Z. L. Water-Solid Surface Contact Electrification and Its Use for Harvesting Liquid-Wave Energy. *Angew. Chem., Int. Ed.* **2013**, *52*, 12545–12549.
29. Lin, Z. H.; Cheng, G.; Lee, S.; Pradel, K. C.; Wang, Z. L. Harvesting Water Drop Energy by a Sequential Contact-Electrification and Electrostatic-Induction Process. *Adv. Mater.* **2014**, *26*, 4690–4696.
30. Lin, Z. H.; Cheng, G.; Wu, W.; Pradel, K. C.; Wang, Z. L. Dual-Mode Triboelectric Nanogenerator for Harvesting Water Energy and as a Self-Powered Ethanol Nanosensor. *ACS Nano* **2014**, *8*, 6440–6448.
31. Liu, H.; Szunerits, S.; Pisarek, M.; Xu, W.; Boukherroub, R. Preparation of Superhydrophobic Coatings on Zinc, Silicon, and Steel by a Solution-Immersion Technique. *ACS Appl. Mater. Interfaces* **2009**, *1*, 2086–2091.
32. Washabaugh, A. P.; Zahn, M. Flow Electrification Measurements of Transformer Insulation Using a Couette Flow Facility. *IEEE Trans. Dielectr. Electr. Insul.* **1996**, *3*, 161–181.
33. Eric, M.; Thierry, P.; Gerard, T. Space Charge Density in Dielectric and Conductive Liquids Flowing Through a Glass Pipe. *J. Electrost.* **2001**, *51—52*, 448–454.
34. Li, X. H.; Yu, X. M.; Zhang, D. C.; Li, Z. H.; Xu, W. H. A Micro Diffuser/Nozzle Pump with Fins on the Sidewall. *Transducers 07, Int. Conf. Solid-State Sens. Actuators* **2007**, 2207–2210.
35. Katayama, K.; Uchimura, H.; Sakakibara, H.; Kikutani, Y.; Kitamori, T. *In situ* Microfluidic Flow Rate Measurement Based on Near-field Heterodyne Grating Method. *Rev. Sci. Instrum.* **2007**, *78*, 083101.
36. Lam, E. W.; Cooksey, G. A.; Finlayson, B. A.; Folch, A. Microfluidic Circuits with Tunable Flow Resistances. *Appl. Phys. Lett.* **2006**, *89*, 164105.
37. Mukhopadhyay, S.; Roy, S.; D'Sa, A.; Mathur, A.; Holmes, J.; McLaughlin, A. Nanoscale Surface Modifications to Control Capillary Flow Characteristics in PMMA Microfluidic Devices. *Nanoscale Res. Lett.* **2011**, *6*, 411.
38. Åkerlöf, G. Dielectric Constants of Some Organic solvent-water mixtures at various temperatures. *J. Am. Chem. Soc.* **1932**, *54*, 4125–4139.
39. Jana, N. R.; Gearheart, L.; Murphy, C. J. Wet Chemical Synthesis of High Aspect Ratio Cylindrical Gold Nanorods. *J. Phys. Chem. B* **2001**, *105*, 4065–4067.
40. Zhang, W.; Lin, S.; Wang, C.; Hu, J.; Li, C.; Zhuang, Z.; Zhou, Y.; Mathies, R. A.; Yang, C. J. Pmma/Pdms Valves and Pumps for Disposable Microfluidics. *Lab Chip* **2009**, *9*, 3088–94.